Numerical Methods in Civil Engineering, 7-2 (2022) 50-60

Numerical Methods in Civil Engineering

Journal Homepage: https://nmce.kntu.ac.ir/

Numerical analysis of reinforced concrete beam-column joints without transverse reinforcement

Freydoon Rezaie*, Seyed Mohammad Farnam, and Sadegh Pour Bahar*****

ARTICLE INFO

RESEARCH PAPER

Article history:
Received:
November 2021.
Revised:
May 2022.
Accepted:
May 2022.

Keywords:
Validation Analysis;
Nonlinear Finite Element Method;
Beam-Column corner Joints;
Transverse Reinforcement

Abstract:

This research uses a nonlinear finite element analysis to evaluate and validate two experimental specimens. The Hognestad stress-strain model is used to express the uniaxial compressive behavior of concrete to define three-dimensional concrete in the ABAQUS software, and the linear model is utilized to introduce its tensile behavior. Furthermore, a bilinear model with kinematic hardening is used to simulate the behavior of the steel. Both corner and knee joints, including transverse beams and slabs, are investigated using experimental results from different aspects, including force-displacement hysteresis diagram, the effect of stiffness deterioration, fractural mode, energy absorption rate, and the contour of fracture, and von Mises stress. This study examines two different models which present the predictive modeling, so it is shown that the current model has remarkable power and high reliability by taking into account some important effective parameters in the modeling, such as vulnerable regions, design codes defects, the impact of concrete confinement in large plastic strains, and local buckling. To sum up, this research not only provides a reliable model with the lowest inaccuracy in the study of concrete corner beam-column under seismic load but also presents a simplification in the modeling process that highly reduces analysis time.

1. Introduction

This study investigates the behavior of reinforced concrete corner beam-column joints affected by cyclic lateral loads in one and two directions using nonlinear finite element analysis. Reinforced concrete buildings constructed prior to the seismic design regulations adopted by design codes have many design imperfections that their damage in earthquakes has resulted in irreversible losses and financial costs. Such structures exist throughout seismic regions of the world, and their risk for seismic events is not fully understood.

Beam-to-column connections are the critical components in the deformation capability of these structures since they play a key role in the performance of structural systems.

In recent decades, seismic vulnerability of beam-to-column external connections has been observed in earthquake field reports. In many cases, the failure of the joint has been identified as a contributing factor to the loss of the structure's load-bearing capacity [1-4].

External corner joints usually suffer greater damage than internal joints during seismic events. Engindeniz cites some of the most important reasons for this issue: (a) these joints have the least confinement between building connections since the beams are connected only from two sides; (b) the axial load on the outer columns is usually lower than on the inner columns, and this load can be reduced due to the cyclic behavior of the earthquake lateral load; (c) the asymmetric presence of the beam and slab in the outer joints results in increased torsion conducted from the beams to the joint; (d) biaxial bending in the column due to the combined effect of two perpendicular frames results in increased axial stress in the inner and outer corners of the column in the joint area; and (e) higher forces are applied to the external joints due to their further distance from the center of stiffness during an earthquake and the structure complete torsion [4-5]. In 2008,

* *Associate Professor, Department of Civil Engineering, Faculty of Engineering, Bu-Ali Sina University, Hamedan, Iran. Email: frezaie@basu.ac.ir.*

** *Corresponding author, Assistant Professor, Department of Civil Engineering and Architect, Faculty of Engineering, Raja University, Qazvin, Iran. Email: M.Farnam@raja.ac.ir.*

*** *Master of Civil-Structural Engineering, Department of Civil Engineering, Faculty of Engineering, Bu-Ali Sina University, Hamedan, Iran.*

Manfredi et al. simulated a beam-column unidirectional interconnection response to evaluate the resistance deterioration. The other goal of this study was to accept or reject the use of connection shear as an indicator to evaluate the performance of the joint [6]. In 2009, Lee et al. investigated the cyclic response of a unidirectional internal beam-column joint with insufficient steel bars in both experimental and numerical approaches. In this study, several specimens were modeled as simple beam-column joints, and some others consisted of slabs and transverse beams. The beams were extended to the effective width of the slabs and were designed to simulate the confinement caused by transverse beam connections [7]. In 2011, Akguzel conducted a comprehensive study on numerical and experimental results of corner joints without transverse reinforcement and any slab. He examined a series of knee joints refined by FRP layers without transverse reinforcement under simulated seismic loads. In this research, joints were affected by one-way and two-way lateral loads and the column's axial static and dynamic load. Furthermore, due to nominally identical details of the rebar in both one-way and two-way models, the effect of these loading and also the effect of higher joint confinement were evaluated and compared [8]. In a related paper by Deaton in 2013, a set of external corner beam-column joints with insufficient bars was numerically investigated using the DIANA finite element software [9]. In this study, corner joints were loaded alternatingly. To simulate the concrete behavior, the total strain rotating crack model, a nonlinear orthotropic model proposed by Selby and Vecchio (1996 and 1997), was used [10-12].

Despite the advances presented in the studies, the behavior of joints without transverse reinforcement located at the corner of the building under two-way loading is still not fully understood, and various factors must be investigated to determine the strength and deformability of these joints. The American Concrete Institute, in ACI 352, calls for further research specifically on the behavior of existing joints with non-seismic detail as follows: "Joints in the structures constructed before extending the design criteria in the current code do not satisfy the current needs and must be studied comprehensively to give engineers a better view of how these joints can be rehabilitated".

2. Numerical modelling

In this research, one of the connections tested by Pantelides et al. [13] is modeled and evaluated using the ABAQUS finite element software. In this paper, the push-over analysis is used to model hysteresis load as far as possible well. Moreover, this analysis in ABAQUS is followed by the concrete damaged plasticity technique to better illustrate the connection's behavior. This connection has several defects, most notably the lack of transverse rebar in the coupling core. The connection loading is applied in a cyclic mode and two steps. The second part of the work involves the analysis of a knee joint with a slab which is validated by the experimental results of Engindeniz [5]. This connection contains four major failures and is supposed to have the worst seismic conditions. Both connections are designed by ACI 318-19 [14], and this code has been formulated before adopting the seismic criteria.

2.1 Material behavioural models

In this paper, the concrete damaged plasticity model is used to simulate nonlinear concrete behavior by Farnam and Rezaie [15-19]. To express the compressive behavior of concrete, the Hognestad compression model [20] is used in the ABAQUS finite element software [21]. Considering concrete's stress-strain model, concrete under tensile stress exhibits some nonlinear behavior, although the behavior of concrete is linear up to 50% of its tensile strength. The tensile behavior of concrete is such that even after reaching the maximum tensile strength, the concrete can still withstand some of the tensile stresses perpendicular to the crack; this phenomenon is called residual tensile stiffness. In this study, by neglecting these small values, a simple linear model is used to model the tensile behavior of concrete. A bilinear diagram with kinematic hardening is used to simulate the behavior of steel. Initial studies showed that joint behavior is not highly sensitive to steel behavior. In addition, the element embedding technique is also used to model the bonding behavior of longitudinal and transverse bars. In this technique, the degrees of freedom of embedded elements (bars) are bound to the degrees of transitional freedom of the host concrete elements. As such, it is considered to be a perfect bond for the bars.

For meshing the concrete part, the C3D8R element is used, and for the longitudinal bars and stirrups, where only the axial force is present and no moment is transferred, the T3D2 three-dimensional truss element with elastoplastic behavior is assigned.

2.2 Examined parameters

In this study, the relative displacement-force diagram, stiffness deterioration, loss of energy during loading, and shear stress in the coupling core are investigated for each joint. For both joints, the load is applied as force or displacement to the endpoints of the beam, and the displacement and the corresponding force are measured, respectively, so that the relative displacement-force diagram can be plotted. The loss of energy in each cycle is equal to the area enclosed by the force-displacement diagram of that cycle (Figure 1). The stiffness deterioration in each cycle is calculated from the force-displacement graph using

Equation (1). In Figure 1, the parameters used in Equation (1) are presented.

$$K_{ppn} = \frac{F_{max_n} - F_{min_n}}{X_{max_n} - X_{min_n}} \quad (1)$$

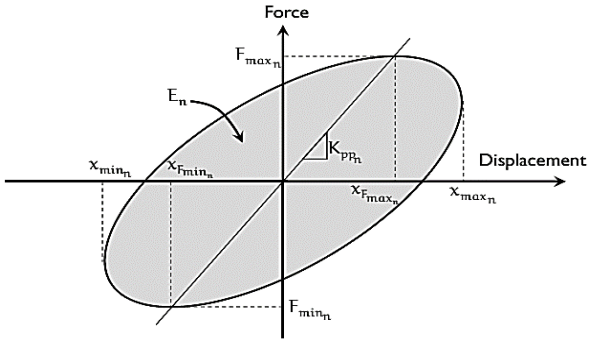

Fig. 1: Stiffness deterioration and the loss of energy in cycle n [5].

The joint of shear stress is defined as the average shear stress imposed on a horizontal surface at the mid-height of the joint. The joint shear in the test is calculated based on the value of external reactions at the end of the beam and columns. If V_b is the applied force to the beam end, it will induce a moment equal to $V_b l_b$ on the connection side, that l_b is the length of the beam considered from the point of load position to the connection side (Figure 2). The induced moment can be substituted by a pair of equal forces named C_b and T_b, with the distance of j_d from each other, as shown in Equation (2). The moment arm, j_d, is usually considered equal to 0.875 of the effective depth of the beam, d. Therefore, the joint horizontal shear force, V_{jh}, can be obtained from Equation (3):

$$C_b = T_b = \frac{V_b\, l_b}{j_d} \quad (2)$$

$$V_{jh} = C_b - V_c \quad (3)$$

Consequently, the shear stress of the joint is calculated by dividing the obtained shear force by the area of the transverse section of the joint in the middle part, as shown in Equation 4. In this equation, h_b and h_c are the beam width and column width, respectively.

$$\tau_{jh} = \frac{V_{jh}}{h_b\, h_c} \quad (4)$$

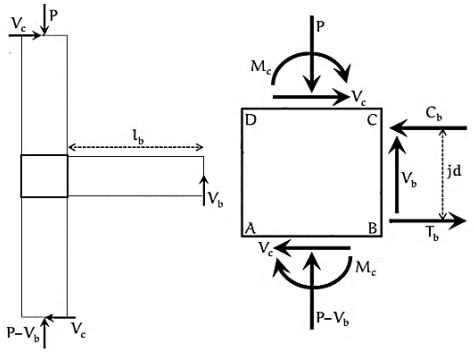

Fig. 2: Equilibrium of the joint and the forces exerted on it.

3. Results of simulated validation models

3.1 The Corner joint

In order to validate the presented model in this study, the corner joint tested by Pantelides et al. [6] has been examined using the finite element method. The geometry, rebar details, boundary conditions, and strength of used steel and concrete are in accordance with the above experimental study. Moreover, the first protocol for this test is defined as the loading equipment and the loading protocol, as shown in Figures 3 and 4, respectively.

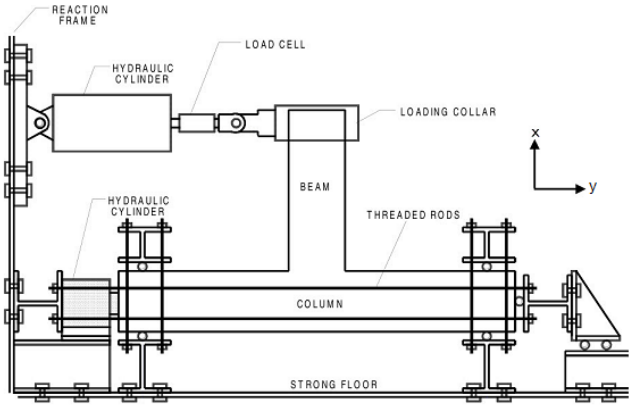

Fig. 3: The loading set-up and equipment.

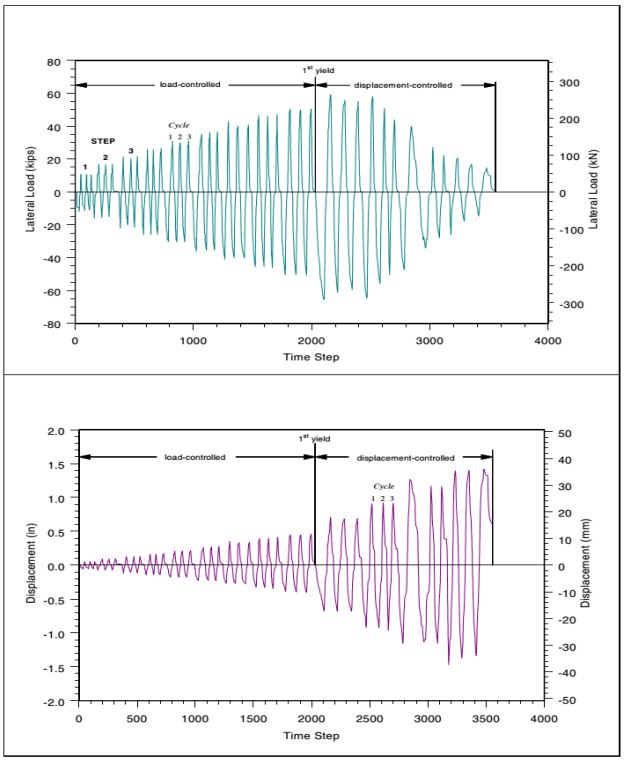

Fig. 4: The loading protocol.

3.1.1 The corner joint details

The geometry and details of the joint of the experimental study are illustrated in Figure 5. The compressive strength of concrete used in the experimental specimen is 41 MPa,

and the yield strength of longitudinal bars of the beams, columns, and stirrups are 454.4, 469.5, and 427.5 MPa, respectively. The column of size 458×305 mm is reinforced by 8 bars with 22-mm diameter, which makes the percentage of longitudinal steel equal to 2.54%. Also, the beam of size 406×305 mm is reinforced by 4 bars with 29-mm diameter in both top and bottom layers. Both the top and bottom steel bars of the beam are embedded using a 90° standard hook. The column's longitudinal bars are also cut and overlapped at exactly 536 mm above the joint core.

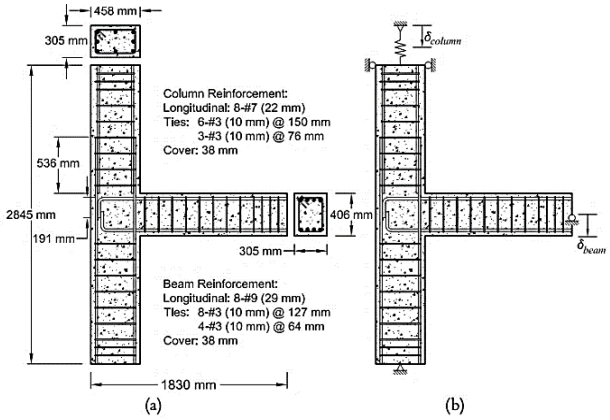

Fig. 5: Geometry, bar details and boundary conditions by Pantelides et al [6].

In this experiment, the column is positioned horizontally, and its two ends are restrained by pinned supports. An initial axial load (P_{ini}) equal to Equation (5) is applied to the column by a hydraulic jack. Changes in axial load are measured by strain gauges embedded in the bars attached to the jack through whom the force is transmitted. As described in the modeling section, to model the joint in the ABAQUS finite element software and for verification purposes, the applied force in the numerical model is applied to the column's end by using a spring and moving its support, as shown in Figure 6.

$$P_{ini} = 0.25 f_c' A_g \quad (5)$$

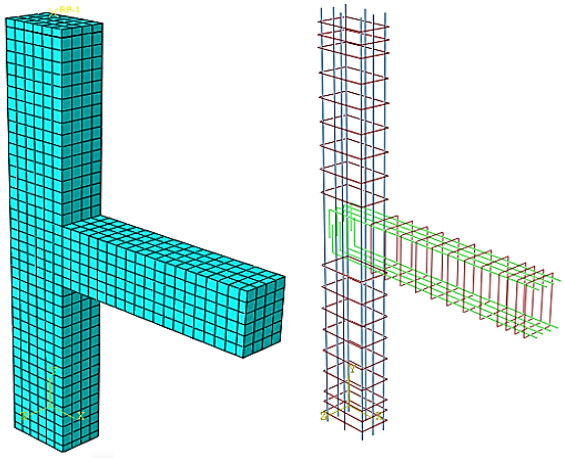

Fig. 6: The corner joint finite element model.

3.1.2 Verification Results

In the experimental model, the load is applied to the end of the beam in two phases by a hydraulic jack moving back and forth in repeated cycles. The load is applied by controlling the force during nine steps and as a displacement control during four steps in the first and second phases, respectively. Each loading step consists of three cycles in the finite element model, and to reduce the computation time, only one cycle per each step is included for the analysis. Figure 7 shows the experimental and numerical specimen loading.

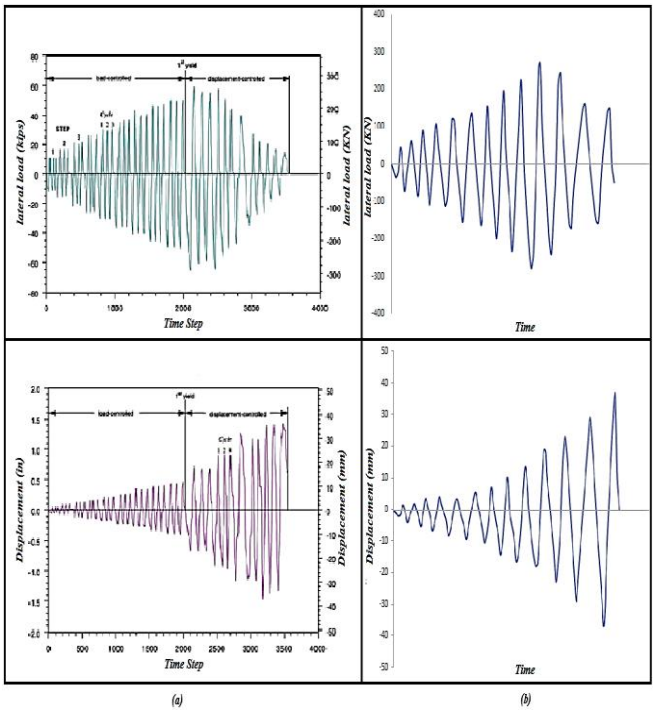

Fig. 7: Force-displacement diagrams of the beam end: a) The experimental result [3] and b) The numerical result.

In Figure 8, the experimental and the present numerical results are shown simultaneously for comparison and verification. The horizontal axis numbers in this diagram represent the relative displacement (drift) obtained by dividing the displacement value of the end of the beam by 1601 mm, the distance from the load effect point to the column's central axis. Figure 9 and Figure 10 can be respectively extracted for the maximum force and displacement using the diagram in Figure 8. According to the graphs, it is found that there is a relatively good agreement between the numerical and experimental results in the early cycles. Nevertheless, in the final cycles, the difference between the maximum beam force in the experimental and numerical models shows that concrete deterioration in the numerical model happens later than in the experimental specimen. This discrepancy can be attributed to the nature of the behavioral model of concrete damaged plasticity and how the bond-slipping behavior of bars is simulated in the numerical model.

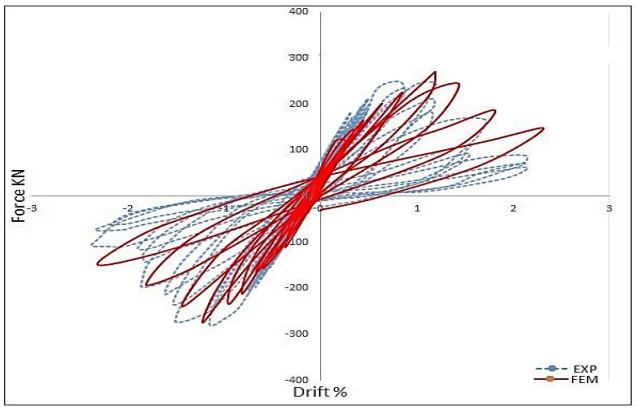

Fig. 8: Relative displacement-force diagram of the beam end in the Pantelides's joint by push-over analysis.

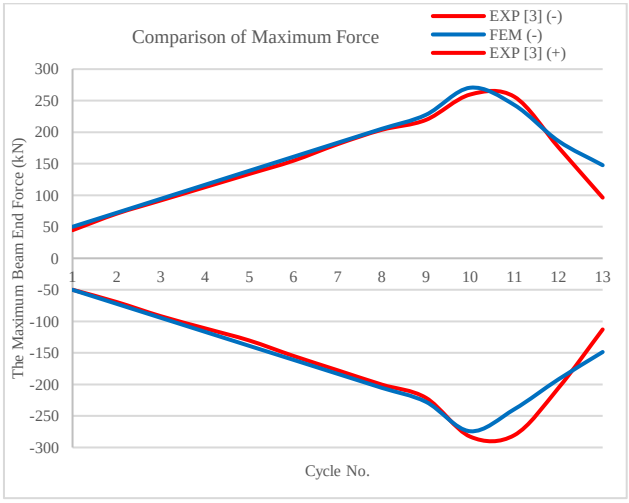

Fig. 9: Comparison of maximum force of beam end in the experimental and numerical studies.

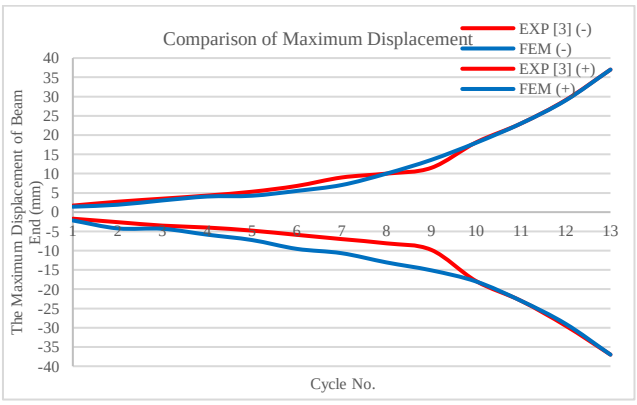

Fig. 10: Comparison of maximum displacement of beam end in the experimental and numerical studies.

The stiffness deterioration in the experimental and numerical results is shown in Figure 11. It can be observed that in the first cycle, the stiffness of the numerical model is slightly higher than that of the experimental specimen. However, in the subsequent cycles, the numerical model shows less stiffness than the experimental specimen due to the higher displacement. Eventually, in the final cycle, the stiffness of the numerical model becomes more than the specimen. This difference in stiffness deterioration can be attributed to the same cases as previously mentioned.

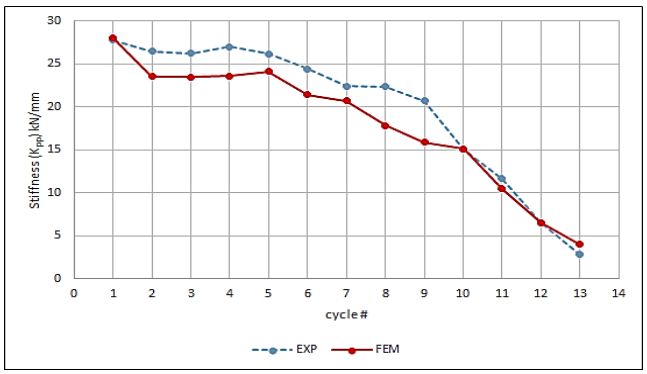

Fig. 11: Stiffness deterioration in the experimental and numerical results for the joint tested by Pantelides et al.

Figure 12 shows the total amount of energy loss until the nth cycle for the experimental specimen and numerical model. As seen, up to the 9th cycle in the first loading stage, the energy loss is small due to the low vibrations. However, in the subsequent cycles, as the beam end displacement increases, the energy loss in the specimen and numerical results become higher. Also, in the last cycle, the energy loss in the numerical model is greater than in the specimen, but due to the greater force in the numerical model than in the experimental specimen, the enclosed area in this cycle is expected to increase.

The maximum nominal shear stress values of the finite element model compared to the experimental specimen are shown in Figure 13. The maximum nominal shear stresses in both models have occurred in the negative displacement of the 11th cycle, with the experimental specimen showing the stress of 14% higher than the numerical model. ACI 352 considers the ratio of shear stress to the square root of the concrete's strength to equal one as the boundary for the shear failure of the joint [6]. According to the test and model results, the joint failure mode is a shear failure.

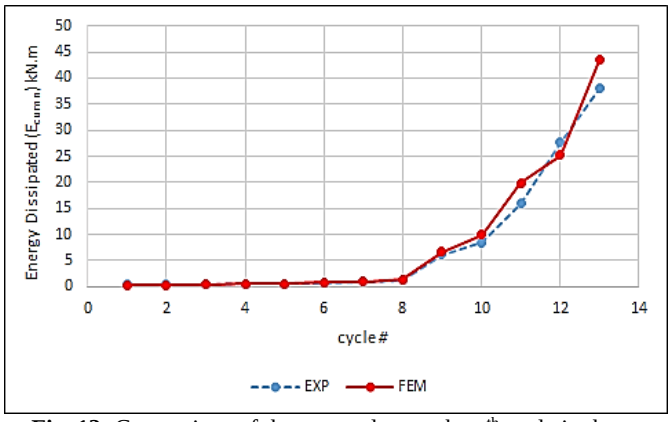

Fig. 12: Comparison of the energy loss to the nth cycle in the experimental specimen and numerical model for the joint tested by Pantelides et al.

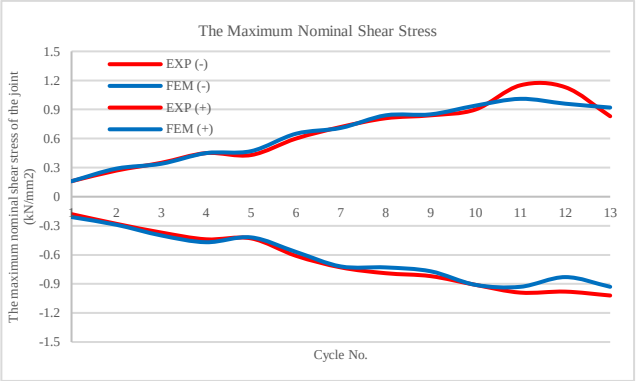

Fig. 13: Nominal shear stress in the joint tested at Pantelides joint.

Figure 14 illustrates the von Mises stress contour in the last joint loading cycle. It is observed that except for the supports where relatively rigid components have been used to prevent the concrete's crushing, the beam's connection area and the joint core also bear a great amount of stress.

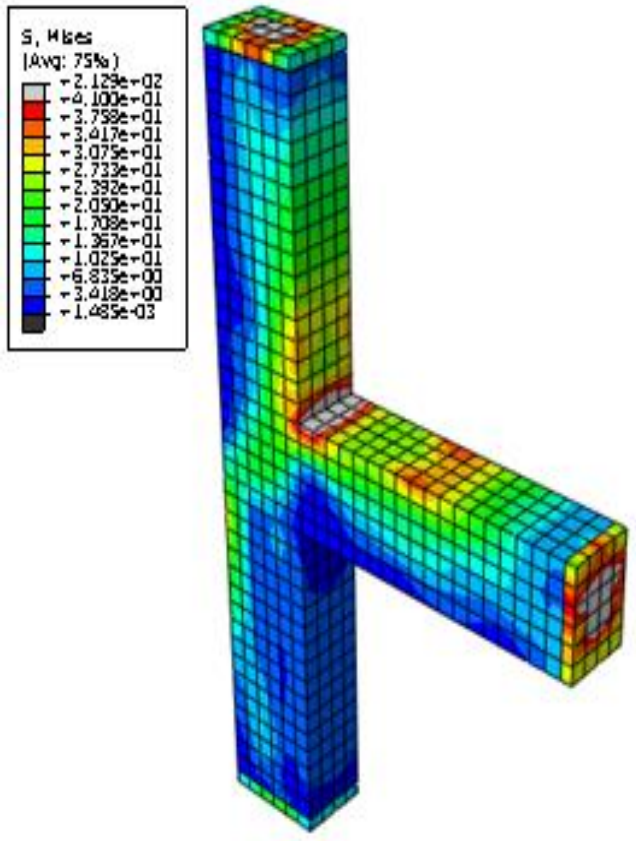

Fig. 14: Von-Mises stress contour for concrete in the last loading cycle.

Moreover, the contour of the plastic strains is displayed in Figure 15, indicating the occurrence of cracks and fractures at the concrete surface compared to the specimen. It is found that the finite element model can predict joint behavior in accordance with the experimental results.

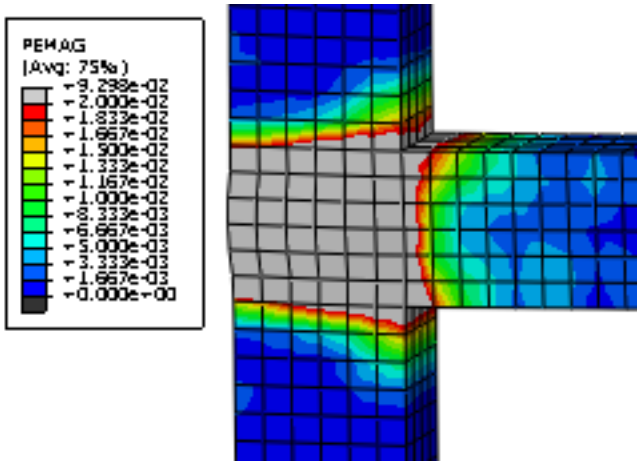

Fig. 15.a)

Fig. 15.b)

Fig. 15: a) Contour of plastic strains in the numerical model, b) Failure of the experimental specimen [6].

3.2 The knee joint

As for the second part of the modeling, a knee joint including a slab with four Seismic failures is investigated. This joint was evaluated in an experimental test by Engindeniz [5]. This connection and its main directions are shown in Figure 16. This connection is the No. 1 example of a series of connections tested by Engindeniz and is designed per ACI 318-63. In the designing process of this joint, as one of the most important seismic failures, the principle of the strong-column weak-beam has been deliberately violated; the ratio of the total flexural strength of the column to the connected

beams in both main directions, therefore, is considered approximately equal to 0.9. Other defects in these models include the lack of transverse rebar in the coupling core, inadequate embedment length of the beam's lower longitudinal bars in the coupling core, and the inadequate length of the overlap in the column's longitudinal bars just above the joint.

Fig. 16: The connection tested by Engindeniz and its defined directions [5].

3.2.1 The knee joint details

The specimen's dimensions and bar details are shown in Figure 17. The column's dimensions are 356×356 mm (14×14 inches), and it is reinforced by a pair of rebar with 16 mm of diameter at each corner. The bars are overlapped just above the connection with a length of 320 mm (12.5 inches). The beam has 305 mm width and 508 mm depth (12×20 inches), and its upper layer is reinforced by 6 bars with 19 mm of diameter and 3 rebars with 19 mm of diameter in its lower layer. The beam's upper bars are restrained by standard 90° hooks in the core, while the beam's lower reinforcements inside have been cut in the core and are restrained directly inside the connector for only 152 mm (6 inches). Both beams are modeled exactly the same, but in order to avoid the interference of the bars in the core, the position of the longitudinal bars of the beam in the X direction is 19 mm upper than the longitudinal bars of the beam in the Y direction (equal to the diameter of a single bar). Steel bars of size 10 mm are chosen as the slab bars and all transverse bars. The slab thickness is equal to 127 mm, and the distances of bars from each other in the upper and lower layers of the slab are 305 mm (12 inches) and 610 mm (24 inches), respectively. During the test, the concrete strength of the lower column, joint core, beams, and slab was equal to 25.8 MPa, while the upper column concrete strength was 34.1 MPa. The yield stress of bars 10, 16, and 19 mm is equal to 367, 352, and 315 MPa, respectively.

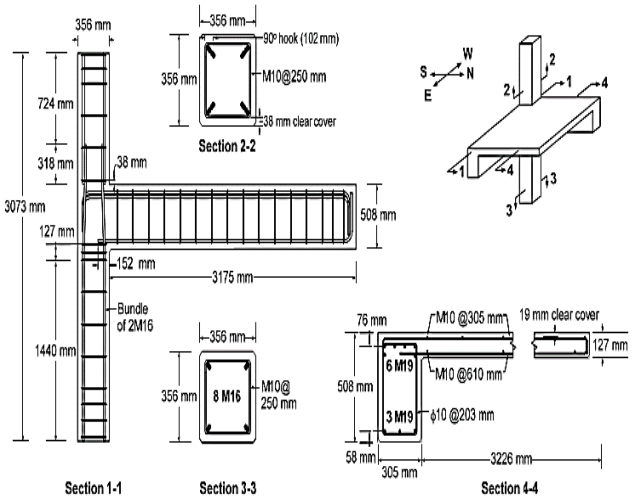

Fig. 17: Details of the bars in the connection tested by Engindeniz [5].

The loading of the joint is carried out as a displacement control at four displacement levels to the points at the end of the beams. The distance of the load effect point from the central axis of the column is equal to 3050 mm. In the numerical model, reduced cycles reduce the computation time (Figure 18).

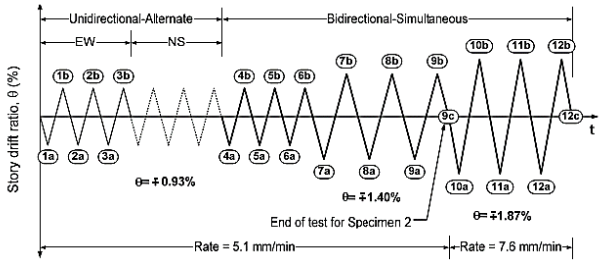

Fig. 18. Loading history of the connection tested by Engindeniz [5].

3.2.2 Results and validation of the knee joint

In this study, the models used were modeled by the Concrete Damaged Plasticity technique of the ABAQUS software in push-over analysis. As a result, in both Figure 19 and Figure 20, the hysteresis force-relative displacement diagrams obtained from the finite element analysis are illustrated in comparison with the experimental results for the knee joints. The maximum amount of forces obtained for the joint tested by Engindeniz in the EW and NS direction beams are listed in Figure 21 and Figure 22.

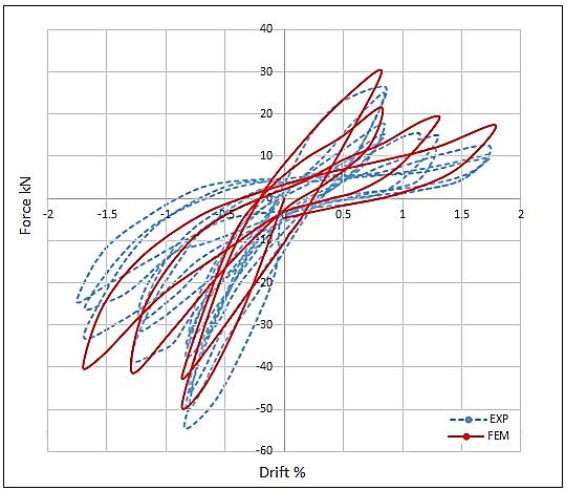

Fig. 19: Force-displacement diagram for EW direction beam by push-over analysis.

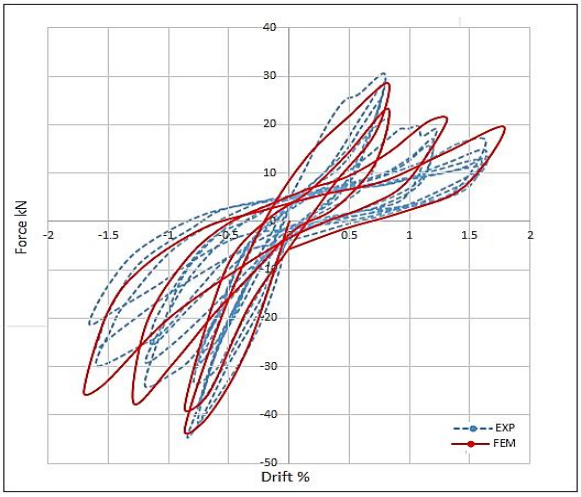

Fig. 20: Force-displacement diagram for the NS direction beam by push-over analysis.

The lowest and highest ratios of force from numerical analysis to the experimental result (FEM/EXP) for the beam in the EW direction occur in the negative direction of the first cycle and the positive direction of the fourth cycle, equal to 0.9 and 1.33, respectively. These minimum and maximum ratios for the beam in the NS direction also occur in the same cycles and directions, with values of 0.93 and 1.2, respectively.

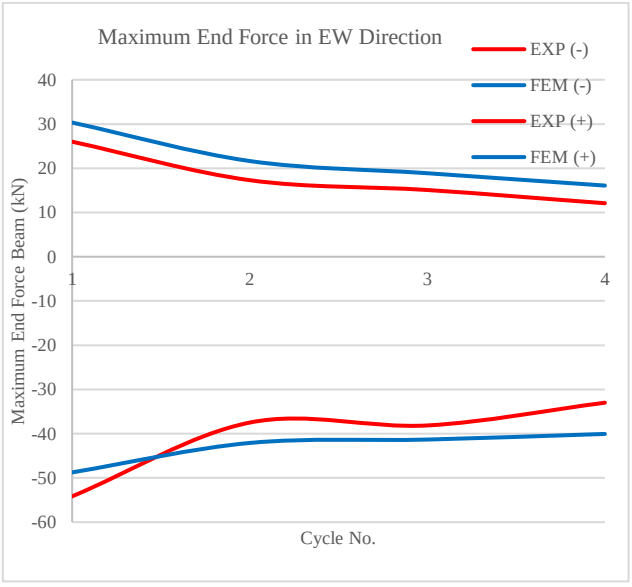

Fig. 21: Maximum beam end forces in the EW direction.

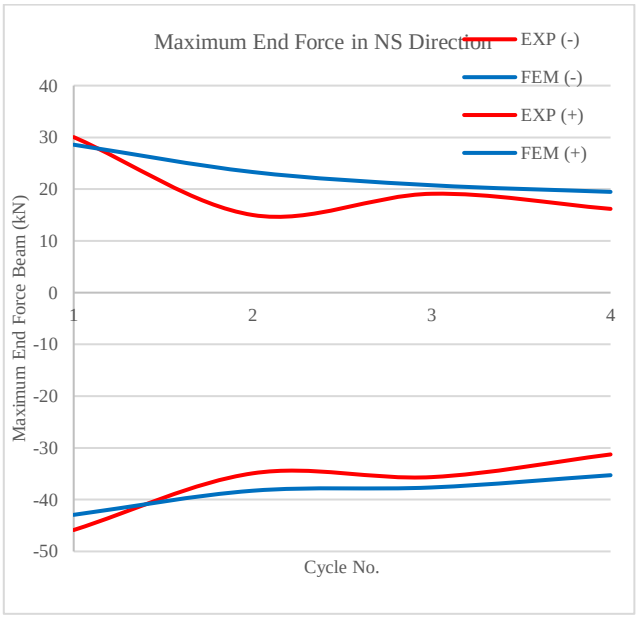

Fig. 22: Maximum beam end forces in the NS direction.

We can show the stiffness deterioration during loading using the tables above and Equation (4). The stiffness of the joint in each cycle is calculated using Equation (4), which is illustrated in comparison with the experimental results in both Figure 23 and Figure 24. It is observed that in both directions except for the first cycle, in other cycles the stiffness in the numerical model is higher than the specimen.

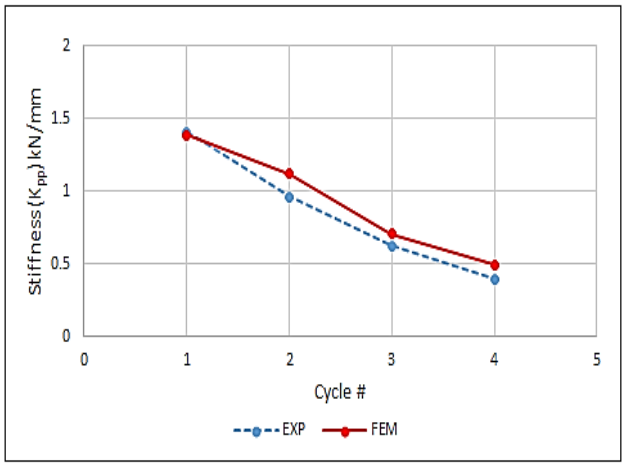

Fig. 23: Stiffness deterioration in the test and numerical models for the EW direction.

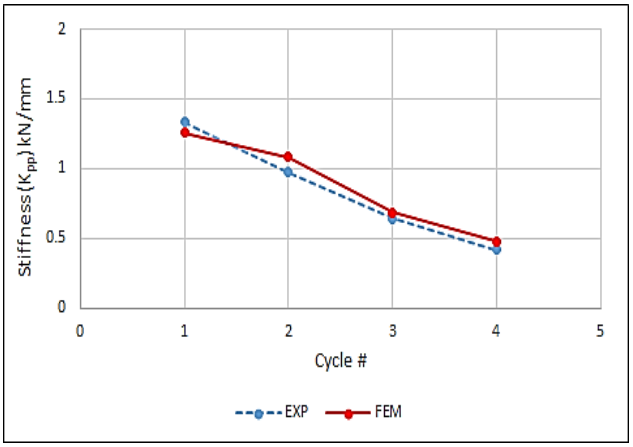

Fig. 24: Stiffness deterioration in the experimental and numerical models for the NS direction.

The energy loss in each cycle for the numerical and specimens is shown in Figure 25. In the first three cycles, less energy is lost in the numerical model, but by the end of the loading, the energy loss in the numerical and specimens is approximately equal.

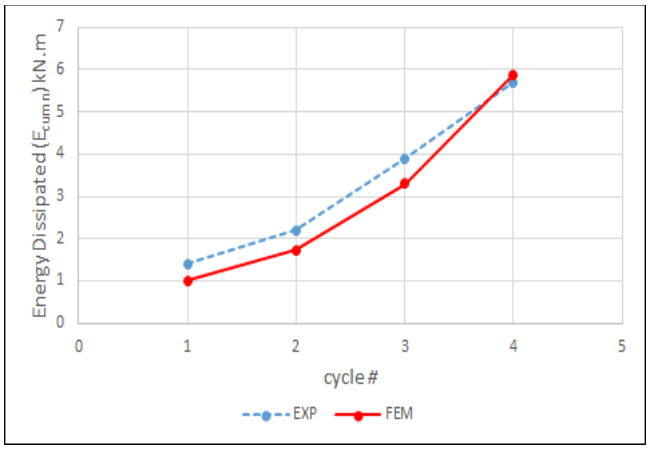

Fig. 25: Total energy loss to the n^{th} cycle for the joint tested by Engindeniz.

The maximum nominal shear stress values of the finite element model compared to the experimental specimens for the EW and NS directions are shown in Tables 1 and 2. The maximum shear stress values in the test and numerical results occur in the first cycle for both directions. Therefore, there is a contradiction between the shear stress of the joint and the displacement direction, so when the displacement is downward in the negative direction, the shear stress is positive and upward; however, this can be expected due to the moment induced to the joint core.

Table. 1: Maximum nominal shear stress in the EW direction in the connection tested by Engindeniz

				Maximum nominal shear stress	
	Cycle No.	Relative displacement (%)	Direction	EXP	FEM
EW	1	0.93	-	0.35	0.40
			+	-0.45	-0.51
	2	0.93	-	0.26	0.25
			+	-0.29	-0.26
	3	1.40	-	0.21	0.25
			+	-0.30	-0.27
	4	1.87	-	0.19	0.21
			+	-0.25	-0.22

Table. 2: Maximum nominal shear stress in the NS direction in the connection tested by Engindeniz.

				Maximum nominal shear stress	
	Cycle No.	Relative displacement (%)	Direction	EXP	FEM
NS	1	0.93	-	0.39	0.14
			+	-0.40	-0.38
	2	0.93	-	0.30	0.33
			+	-0.29	-0.24
	3	1.4	-	0.28	0.33
			+	-0.29	-0.25
	4	1.87	-	0.23	0.28
			+	-0.25	-0.21

In Figure 26, the von Mises stress contour for the inner corner of the joint is shown. It is observed that the inner corner of the joint suffers the most stress due to the bending stress induced in the joint core because of the displacements of the beam ends.

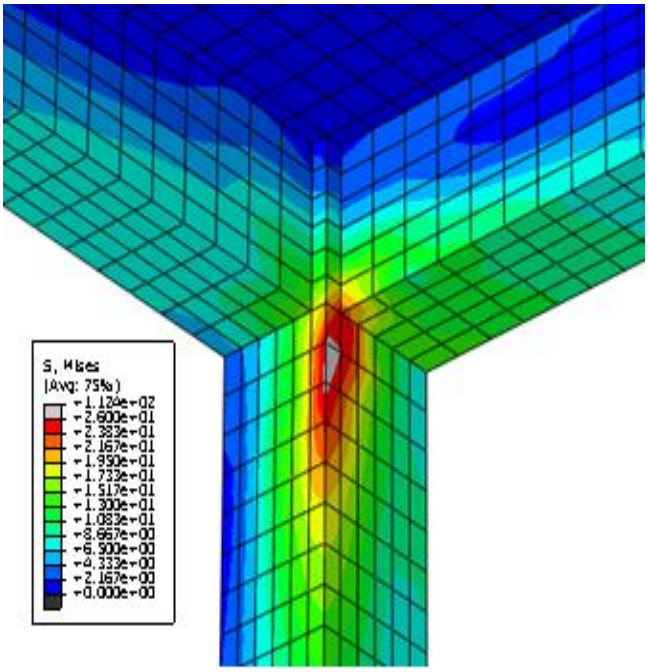

Fig. 26: Von Mises stress contour in the final loading cycle for the inner corner of the connection.

Figure 27 also displays the contour of the plastic strains showing the occurrence of crack and failure on the concrete surface compared to the specimens. Again, this image illustrates that the finite element model can predict the joint behavior very well.

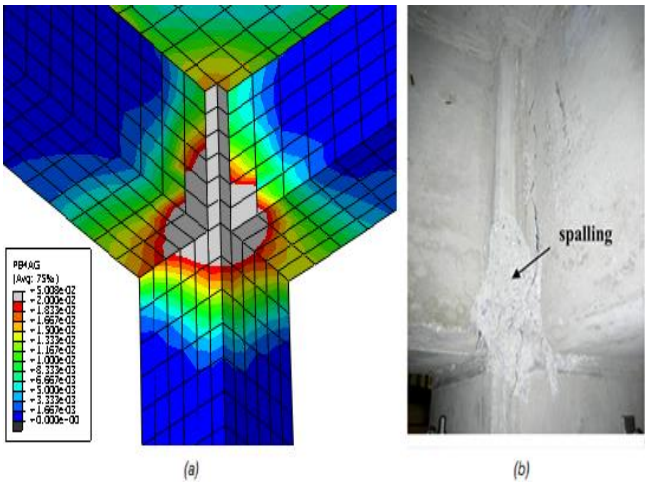

Fig. 27: a) Contour of plastic strains in the numerical model, b) Internal corner failure in experimental specimens [5].

4. Conclusion

This paper studied two different experimental approaches to provide a strong and reliable numerical model for the corner concrete beam-column connection without transverse reinforcement. In this paper, the behavior of two knee concrete joints was investigated. The first joint was loaded in two phases and validated using Pantelides et al.'s results. The shear failure was identified as the main failure mode for this connection. The second joint consists of a transverse beam and a slab, verified using Engindeniz's results. The most important results of this study are as follows:

- The reduction of the number of loading cycles in numerical models does not significantly affect the results, and the load magnitude or the displacement is more effective than the number of repetitions of cycles. Therefore, it is recommended that special attention be paid to the confinement of the connecting core in knee joints. The internal corner of the joint, in addition to the confinement of the cores, should be considered.
- Even though the selected behavior of concrete has some defects, it is an efficient model for concrete modeling under cyclic loads.
- In the early loading cycles, there is a relatively complete agreement between numerical and experimental results. For example, the force ratio of the beam in a numerical model to the test for the corner joint in the initial loading cycle is less than 13%, although, in the last loading cycle, this ratio increases up to 50%. This discrepancy in the last cycle can be attributed to the nature of the selective behavioral model in delaying concrete deterioration and the weakness of the embedded element technique in restraining the bars.
- In the present study, due to the selected behavioral model for concrete and the use of the embedded element technique for the bars' bonding, in the final loading cycles, the fore-relative displacement diagram always shows more force in the numerical model than in the specimen.
- Stiffness deterioration in initial cycles in both numerical models and specimens indicates a good agreement. However, in the last cycles, the stiffness of the numerical model is higher than the specimen; in fact, the comparison of the stiffness in the refined and unrefined models illustrates that the stiffness in the refined models in the same cycles is significantly different from the unrefined models. In addition, in the refined models, the stiffness deterioration occurs in a delay.
- Shear failure is identified as the fracture mode for the joint tested by Pantelides et al. Nevertheless, in the joint tested by Engindeniz, in the experimental test, the deterioration of not only bars' bond but also their slipping is reported as the main cause of the fracture. The numerical model in this study is in exact agreement and illustrates both different fracture mechanisms, except for the delays in the fracture due to the embedded elements technique.

The study also provided a prediction method with different effects, including vulnerable points, designing code weaknesses, the effect of concrete confinement on the occurrence of large plastic strains, cracking, and local

buckling. As a result, the explained model in this paper has significant strength and a high degree of confidence in conducting numerical research in this field.

References

[1] Sezen, H., Elwood, K., Whittaker, A., Mosalam, K., Wallace, J., Stanton, J. (2000). Structural engineering reconnaissance of the August 17, 1999, Kocaeli(Izmit), Turkey, earthquake. PEER Report 2000/09, Pacific Earthquake Engineering Research Center, University of California, Berkeley, December.

[2] Allam, M. S., Elbakry, H. M. F, Arab, I. S. E. (2018). Exterior reinforced concrete beam column joint subjected to monotonic loading. Alexandria Engineering Journal, 57, 4133–4144.

[3] Attari, N., Yousef, Y. S., Amziane, S. (2019). Seismic performance of reinforced concrete beam–column joint strengthening by FRP sheets. Structures, 20, 353–364.

[4] Obaidat, Y. T., Abu-Farsakh, G. A. F. R., Ashteyat, A. M. (2019). Retrofitting of partially damaged reinforced concrete beam-column joints using various plate-configurations of CFRP under cyclic loading. Construction and Building Materials, 198, 313–322.

[5] Engindeniz, M. (2008). Repair and Strengthening of Pre-1970 Reinforced Concrete Corner Beam-Column Joints Using CFRP Composites. Ph.D. thesis, Georgia Institute of Technology, Atlanta, GA.

[6] Manfredi, G., Verderame, G., Lignola, G. (2008). A F.E.M. model for the evaluation of the seismic behavior of internal joints in reinforced concrete frames. In Proceedings of the 14th World Conference on Earthquake Engineering, Beijing, China.

[7] Lee. S., Kitayama, K., Otani, S., Aoyama, H. (1992). Shear strength of reinforced concrete interior beam-column joints using high-strength materials. Proc. of the Japan Concrete Institute, Japan, 14 (2), 379–384.

[8] Akguzel, U. (2011). Seismic performance of FRP retrofitted exterior RC beam-column joints under varying axial and bidirectional loading, Ph.D. thesis, University of Canterbury, Christchurch, New Zealand.

[9] Deaton, J. B. (2013). Nonlinear finite element analysis of reinforced concrete exterior beam-column joints with non-seismic detailing. Ph.D. thesis, School of Civil and Environmental Engineering Georgia Institute of Technology.

[10] Selby, R., Vecchio, F. (1997). A constitutive model for analysis of reinforced concrete solids. Canadian Journal of Civil Engineering, 24, 460–470.

[11] Selby, R., Vecchio, F., Collins, M. (1996). Analysis of reinforced concrete members subject to shear and axial compression. ACI Structural Journal, 93 (3).

[12] ACI, ACI 352R-02. (2002). Recommendations for Design of Beam-Column Connections in Monolithic Reinforced Concrete Structures. ACI-ASCE Committee 352, American Concrete Institute, Farmington Hills, Michigan.

[13] Pantelides, C., Clyde, C., Reaveled, L. (2002). Performance-based evaluation of reinforced concrete building exterior joints for seismic excitation. Earthquake Spectra, 18, 449–480.

[14] ACI, ACI 318-63. (2019). Building code requirements for structural concrete and commentary. ACI Committee 318, American Concrete Institute, Detroit, Michigan.

[15] Rezaie, F., Farnam, S. M. (2015). Fracture Mechanics Analysis of Pre-stressed Concrete Sleepers via Investigating Crack Initiation Length. Engineering Failure Analysis – Elsevier, 58, 267-280.

[16] Rezaie, F., Bayat, M.. A, Farnam, S. M. (2016). Pre-stressed Concrete Sleepers Sensitivity Analysis for Affective Factors of Longitudinal Crack Prorogation. Engineering Failure Analysis – Elsevier. 66, 385–397.

[17] Farnam, S. M., Rezaie, F. (2019). Simulation of Crack Propagation in Pre-stressed Concrete Sleepers by Fracture Mechanics. Engineering Failure Analysis – Elsevier, 96, 109-117.

[18] Farnam, S. M., Rezaie, F. (2017). Part A- Experimental: Experimental Analysis of Crack Propagation in Pre-stressed Concrete Sleepers by Fracture Mechanics. International Journal of Transportation Engineering, 4 (3), 17-29.

[19] Farnam, S. M., Rezaie, F. (2017). Experimental Analysis of Fracture and Damage Mechanics of Pre-Stressed Concrete Sleepers B70: Part B- Analysis. International Journal of Transportation Engineering, 5 (1), 163-177.

[20] E. Hognestad. Inelastic behavior in tests of eccentrically loaded short reinforced concrete columns. Journal of the American Concrete Institute, 124 (1952) 177–139.

[21] ABAQUS/CAE user's manual, version 6.13. (2013). Hibiit Karlson & Sorensen Inc.